Supplementary Information

Table of Contents

Supplementary Methods

Supplementary Note

Supplementary Figures
- Supplementary Figure 1
- Supplementary Figure 2
- Supplementary Figure 3
- Supplementary Figure 4
- Supplementary Figure 5
- Supplementary Figure 6
- Supplementary Figure 7
- Supplementary Figure 8
- Supplementary Figure 9
- Supplementary Figure 10

Supplementary Tables
- Supplementary Table 1
- Supplementary Table 2
- Supplementary Table 3
- Supplementary Table 4
- Supplementary Table 5
- Supplementary Table 6
- Supplementary Table 7
- Supplementary Table 8

Supplementary Methods

Detailed Quality Control for Whole-Exome Sequencing Data

To ensure the robustness of the rare variant analyses, stringent sample-level quality control (QC) was applied to the whole-exome sequencing (WES) data. Samples were evaluated and excluded if having outlier values in any of the following sequence quality metrics: extreme number of singletons (> 120), abnormal heterozygous-to-homozygous non-reference (Het/Hom) ratios (< 1.35 or > 1.85), deviated transition-to-transversion (Ti/Tv) ratios (< 3.10 or > 3.45), or low overall call rates (< 0.82).

At the genotype level, individual genotypes were set to missing using bcftools (1) if they failed to meet variant-specific quality thresholds. For single nucleotide polymorphisms (SNPs), genotypes were masked if they had a read depth (DP) < 7, a genotype quality (GQ) < 20, or if they exhibited abnormally high depth (DP > 150) combined with a GQ < 95. Additionally, heterozygous SNP calls had to have an alternate allele fraction (AB) between 0.15–0.85. For insertions and deletions (INDELs), filtering criteria were more strictly defined: DP < 10, GQ < 20, or DP > 150 combined with GQ < 95, and an AB between 0.20 and 0.80 for heterozygous calls.

Detailed Quality Control for Genotyping Array Data

Quality control of the Global Screening Array data was performed using PLINK (2). The initial analysis of autosomal SNPs followed these filtering criteria: variant missing rate < 0.02, individual missing rate < 0.1, minor allele frequency > 0.05, and Hardy-Weinberg equilibrium (HWE) $P > 1 \times 10^{-3}$ in controls. Linkage disequilibrium (LD) pruning was conducted using a window size of 50 variants, a step size of 5, and an r^2 threshold of 0.2.

To assess global population stratification, the unrelated cohort was merged with the 1000 Genomes Project reference panels. Merged datasets underwent a separate QC protocol to retain only high-quality common SNPs: variant missing rate < 0.05, individual missing rate < 0.1, MAF > 0.05, and HWE $P > 1 \times 10^{-6}$, followed by strict LD pruning (window size = 50, step size = 5, $r^2 < 0.2$).

Gene-level analysis

For the Japanese-cohort gene-level analysis, qualifying variants were collapsed by individual and gene within each of the three prespecified variant models. Carrier proportions in cases and controls were compared using two-sided Fisher's exact tests, and odds ratios and 95% confidence intervals were derived from the corresponding 2 × 2 tables. Benjamini–Hochberg correction was applied across genes separately within each variant model. *P*-values < 2.5×10^{-6} and *q*-values < 0.05 were considered exome-wide significant and FDR-significant, respectively.

Detailed gene-level meta-analysis

We performed a cohort-stratified gene-level meta-analysis by combining the Japanese cohort with publicly available gene-level summary data from SCHEMA (3) and an independent case-control cohort reported by Chick *et al.* (4). The analysis included 24,248 cases and 97,322 controls from SCHEMA, 4,650 cases and 5,719 controls from the Chick *et al.* cohort, and 3,831 cases and 5,119 controls from the Japanese cohort. Published case-control variant counts and gene-based de novo *P*-values were obtained from Supplementary Data 2 of Chick et al.

In the Japanese cohort, we used all cohort singletons that were absent from the gnomAD v4.1 genomes dataset. PTVs included stop-gain, frameshift, and essential splice-site variants. Missense variants were classified according to MPC scores. Three nested models were evaluated: PTVs alone, PTVs plus missense variants with MPC > 3, and PTVs plus missense variants with MPC > 2. Within each model, qualifying Japanese variants were collapsed by individual and gene using logical unions, such that each individual was counted at most once per gene and model. Case and control carrier counts were then calculated for each gene.

Gene symbols were harmonized across the three data sources before merging, including the mapping of historical gene symbols to their current symbols (e.g., *HIST1H1E* to *H1-4*). For Japanese variants annotated to multiple genes, the first annotated gene was used for the primary gene assignment.

For each gene and model, the SCHEMA, Chick et al., and Japanese cohorts were treated as separate strata in a two-sided Cochran–Mantel–Haenszel (CMH) test. The test statistic was calculated with Yates' continuity correction using the observed 2 × 2 contingency tables. A stratum was excluded only when no qualifying carriers were observed among either cases or controls. No pseudo-counts, including a manual 0.5 cell correction, were added to individual cells. Mantel–Haenszel common odds ratios and 95% confidence intervals were reported when estimable; when no control carriers were observed across the informative strata, the common odds ratio was reported as infinite and the confidence interval as not estimable. For models with a case-control *P*-value ≤ 0.01 and an available corresponding published de novo *P*-value, Fisher's combined probability test was applied, and the smaller of the case-control and Fisher-combined *P*-values was retained. For each gene, the minimum final *P*-value across the three prespecified models was multiplied by three and capped at 1. To assess the extent to which the results depended on de novo evidence, we additionally calculated, for each gene, a case-control-only *P*-value as the minimum CMH *P*-value across the three prespecified variant models, multiplied by three and capped at 1, without integrating de novo evidence. To quantify the contribution of the Japanese cohort, we repeated the CMH analysis after excluding the Japanese stratum while retaining the variant model selected in the full analysis. We calculated $\Delta(-\log10\ P) = \log10(P_\text{without Japanese}/P_\text{full})$,

where *P*_full and *P*_without Japanese denote the CMH *P*-values from the full and Japanese-excluded analyses, respectively, under the same full-analysis-selected variant model. Positive values therefore indicate stronger case-control evidence after inclusion of the Japanese cohort. For the sensitivity assessment of exome-wide significance, the Japanese-excluded *P*-value for this fixed model was derived using the same conditional integration of de novo evidence as in the primary analysis and was multiplied by three to retain the same three-model multiplicity correction.

Benjamini–Hochberg correction was subsequently applied across genes to the primary three-model-adjusted final *P*-values. Three-model-adjusted *P*-values $< 2.5 \times 10^{-6}$ and q-values < 0.05 were considered exome-wide significant and FDR-significant, respectively. Since only gene-level summary counts were available for the published cohorts, cross-cohort variant-level harmonization and reconstruction of ancestry- or sequencing platform-specific strata were not possible.

Detailed Parameters for Copy Number Variant Calling

In WES CRAM files, copy number variants (CNVs) were identified using the eXome-Hidden Markov Model (XHMM) software tool (5). First, the mean read depth for each targeted exon across all samples was calculated using GATK3 DepthOfCoverage, with a minimum mapping quality of 20. Targets were excluded if their GC content was extreme (< 10% or > 90%) or if their sizes were < 10 bp or > 10,000 bp. Additional target filters included extreme mean read depths (< 10x or > 500x). At the sample level, individuals were excluded for abnormal mean read depths (< 25x or > 200x) or highly variable read depths (standard deviation [SD] > 150).

We performed a principal component analysis (PCA) on the mean-centered target read depth matrix. Data normalization was achieved by removing the top principal components that explained the most variance (PVE_mean_factor = 0.7). After calculating sample-level Z-scores and removing targets with extreme variance (SD > 30), the HMM Viterbi algorithm was applied to discover CNV events (deletions and duplications) from the normalized read depth matrix.

Polygenic Risk Score Analysis

Genotype quality control was performed using PLINK (2). Analyses were restricted to autosomal SNPs with standard A/C/G/T alleles. Variants were excluded if they had a genotype missing rate ≥ 0.05, minor allele frequency (MAF) ≤ 0.01, or Hardy–Weinberg equilibrium (HWE) $P \leq 1 \times 10^{-6}$. Individuals with a genotype missing rate ≥ 0.05 were also excluded. All variants located at duplicated genomic positions were removed. After pre-imputation quality control, 343,459 variants and 8,948 of the 8,950 unrelated participants in the WES cohort remained for the PRS analyses.

The target genotypes were converted into chromosome-specific VCF files and aligned to the GRCh37 1000 Genomes Project Phase 3 v5a reference panel using conform-gt. Variant positions, alleles, and strand orientation were checked for consistency with the reference panel. Variants absent from the reference panel or showing inconsistent or ambiguous strand alignment were excluded. Of the 343,459 target variants, 343,168 passed conform-gt alignment; 231 variants were removed because they were not present in the reference panel, and 60 failed strand alignment. The reference-aligned genotypes were subsequently phased and imputed by chromosome using Beagle 5.5 (6, 7) with the GRCh37 1000 Genomes Project Phase 3 v5a reference panel, comprising 2,504 reference samples, and the corresponding GRCh37 genetic maps. Beagle-generated allele dosages were retained for subsequent PRS calculation.

Following imputation, variants were subjected to post-imputation quality control. The analysis was restricted to biallelic SNPs with non-missing variant identifiers. Imputed variants, identified by the presence of the Beagle IMP flag, were required to have an imputation quality score (DR2) ≥ 0.8, whereas directly genotyped variants without the IMP flag were retained without applying the DR2 threshold. For both imputed and directly genotyped variants, the alternate allele frequency in the target cohort was required to be between 0.01 and 0.99, corresponding to MAF ≥ 0.01 for biallelic variants. The number of samples was confirmed to remain unchanged at 8,948 after post-imputation filtering. The filtered chromosome-specific VCF files were converted to PLINK 2.0 (8) PGEN format while retaining imputed allele dosages. A total of 6,359,500 variants across chromosomes 1–22 remained in the post-imputation target dataset.

The primary East Asian (EAS)-derived PRS was generated using PRS-CS (9), which estimates posterior SNP effect sizes under a Bayesian continuous shrinkage prior. Summary statistics from the PGC3 EAS schizophrenia GWAS (10) were used as the discovery dataset, together with the 1000 Genomes EAS linkage disequilibrium (LD) reference panel. The PRS-CS n_gwas parameter was set to 30,515, and the global shrinkage parameter (phi) was set to 1×10^{-2}.

To assess the robustness of the findings to potential sample overlap with the EAS discovery GWAS, a European (EUR)-derived PRS was generated separately using PRS-CS with EUR schizophrenia GWAS summary statistics (11) and the 1000 Genomes EUR LD reference panel. The n_gwas parameter was set to 250,326, with the same phi value of 1×10^{-2}. Thus, PRS-CS was applied independently to the EAS and EUR summary statistics using ancestry-matched LD reference panels. For each ancestry-specific analysis, posterior SNP effect sizes estimated by PRS-CS were applied to imputed allele dosages using the --score function in PLINK 2.0 (8). Chromosome-specific score sums were combined to obtain an individual-level genome-wide PRS. PRS data were available for 8,948 of the 8,950 participants who passed WES quality control (3,829 cases and 5,119 controls).

Supplementary Note

Illustrative clinical observations in two rare-variant carriers

While detailed longitudinal clinical records were unavailable for most of our retrospective cohort, we obtained deep clinical phenotyping for two individuals carrying PTVs in the risk genes *SRRM2* (exome-wide significant) and *PCLO* (FDR-significant, $q = 0.0094$). Notably, the patient carrying the *SRRM2* PTV exhibited severe, treatment-resistant obesity and required recurrent educational hospitalizations for diabetes management. Heterozygous loss-of-function mutations in *SRRM2* are the established cause of an autosomal dominant neurodevelopmental disorder (OMIM: 620439) (12) frequently characterized by significant excess weight and metabolic dysfunction.

Similarly, the patient harboring a PTV in *PCLO*—a gene encoding a presynaptic scaffolding protein (13)—had a documented history of clinical seizures, aligning with its known implication in epilepsy. We recently reported the first evidence that a *de novo* PTV in *BSN* (Bassoon), a structural and functional paralog of *PCLO* (14), causes a severe neurodevelopmental syndrome characterized by ASD, intellectual developmental disorder, and epilepsy (15). The convergence of *PCLO* and *BSN* variants on overlapping neuropsychiatric and seizure phenotypes highlights the vulnerability of the presynaptic cytomatrix. These clinical correlates emphasize that identifying such pleiotropic PTVs not only elucidates the genetic architecture of schizophrenia but may also provide clinically relevant clues to severe neurological and somatic comorbidities, allowing for systematic phenotyping of rare-variant carriers in future studies.

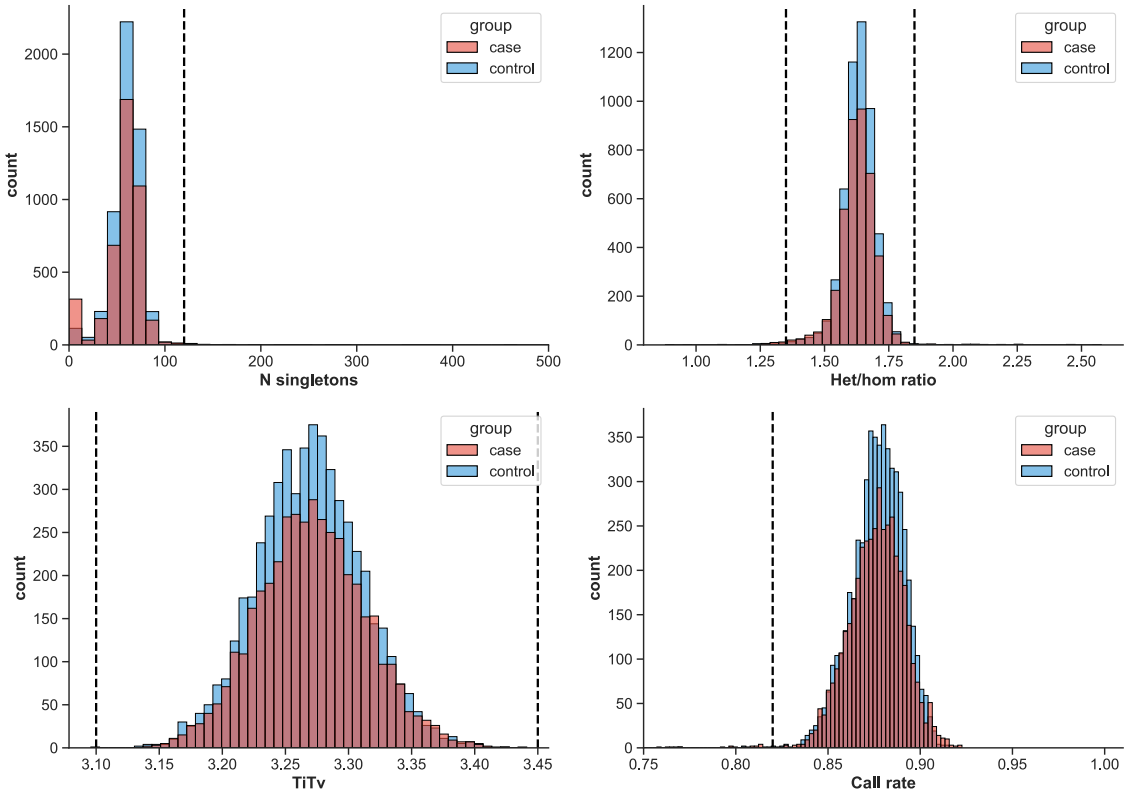

Supplementary Figure 1. Distributions of sample-level QC metrics in the Japanese case-control sample.

Histograms showing the distribution of the number of singleton variants, heterozygous/homozygous variant ratio, transition/transversion ratio, and call rate per sample for schizophrenia cases (red) and controls (blue). Vertical dashed lines indicate the thresholds used to filter outlier samples that failed quality control.

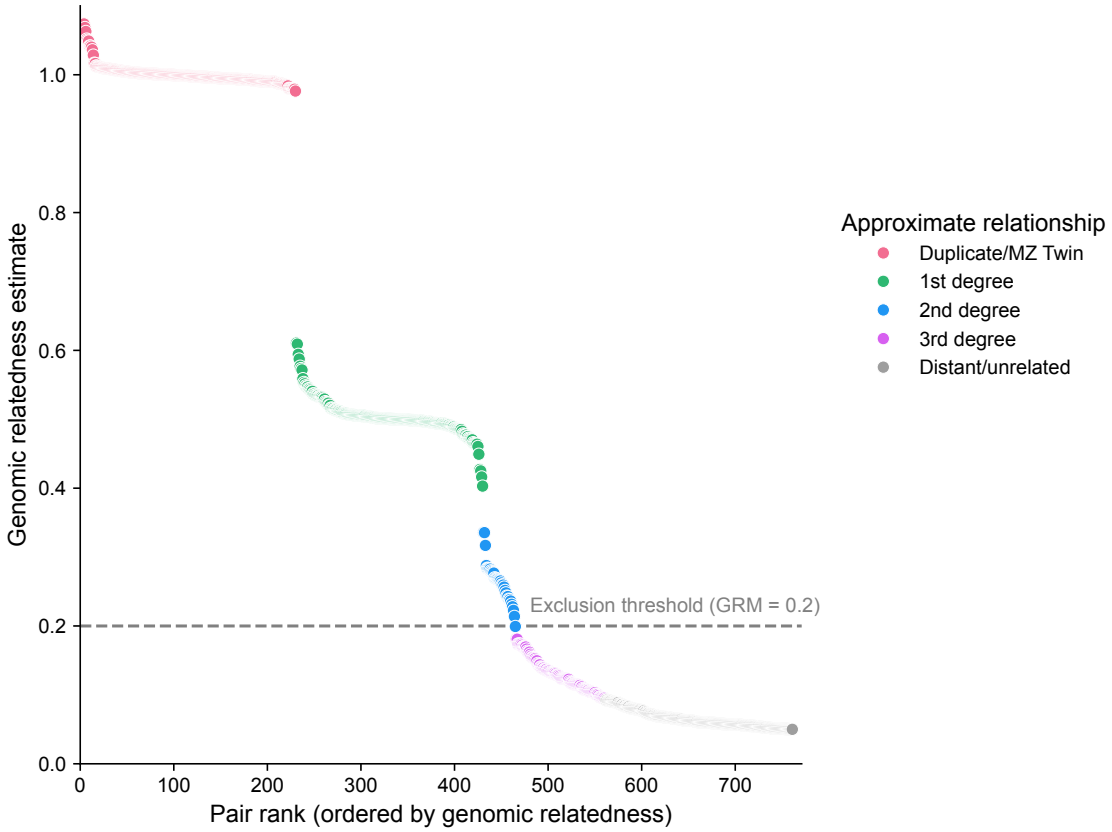

Supplementary Figure 2. Sample relatedness in the Japanese case-control dataset. Pairwise genomic relatedness was estimated using a variance-standardized genetic relationship matrix (GRM) to identify cryptic relatedness. Probable duplicates were first pruned using a GRM cutoff of 0.95, followed by relatedness pruning at a cutoff of 0.2, resulting in an unrelated dataset with no remaining pairs showing a GRM estimate > 0.2 for downstream analyses.

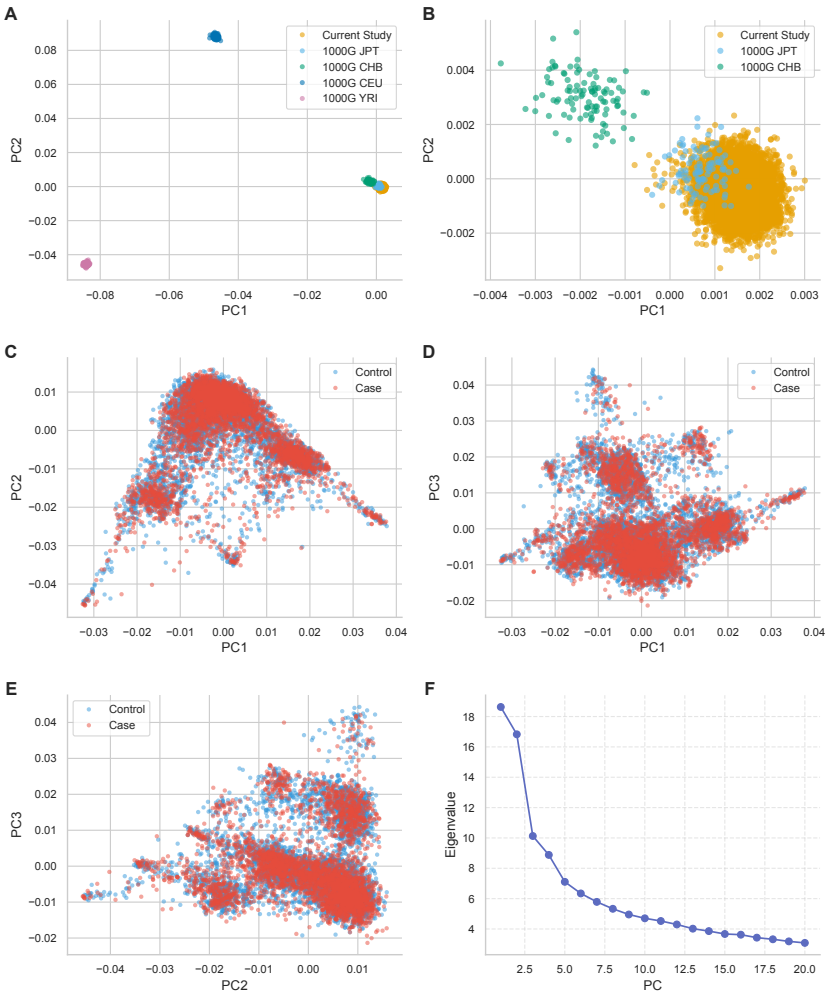

Supplementary Figure 3. Principal component analysis for genetic ancestry inference and population stratification.

(A) Principal component analysis (PCA) of the current study samples alongside reference populations from the 1000 Genomes Project Phase 3 (CEU, YRI, CHB, and JPT). **(B)** A zoomed-in view of the East Asian cluster from panel A, showing that the study samples clustered with the Japanese in the Tokyo (JPT) reference population. **(C–E)** Scatter plots of the top principal components (**C**: PC1 vs. PC2; **D**: PC1 vs. PC3; **E**: PC2 vs. PC3) computed exclusively on the current study dataset. Samples are colored by phenotype (schizophrenia cases in red, controls in blue), showing no evident separation between cases and controls along the plotted principal components. **(F)** Scree plot illustrating eigenvalues across principal components. PCA was conducted on high-quality, LD-pruned, common autosomal SNPs (minor allele frequency > 5%). The top five principal components were extracted and included as covariates in association analyses to account for residual population structure.

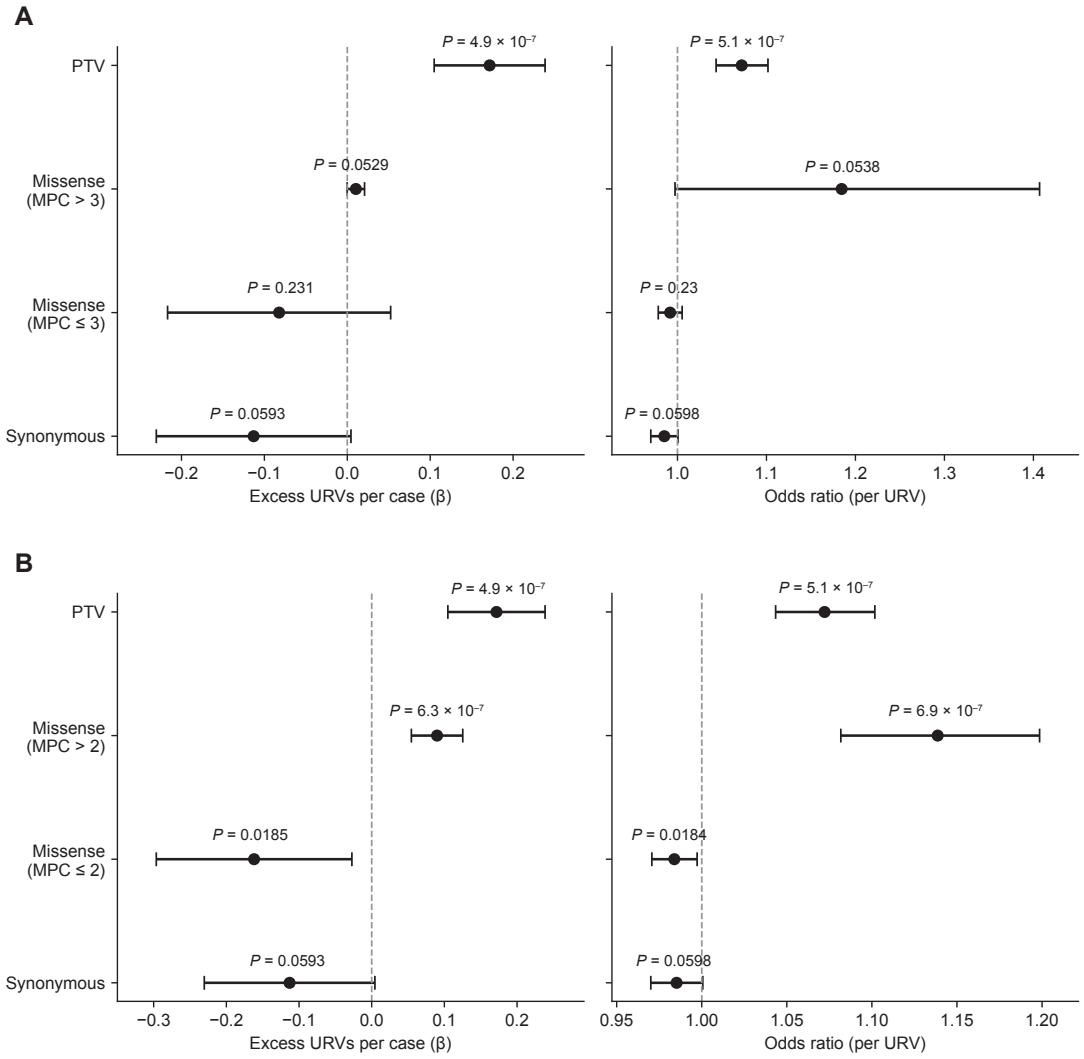

Supplementary Figure 4. Exome-wide burden of ultra-rare variants evaluated under various missense deleteriousness thresholds.

Forest plots illustrate the effect size of URVs across different functional annotation classes. These classes are grouped based on different thresholds for missense variant deleteriousness. (A) Burden of URVs evaluating missense variants with a highly damaging threshold (MPC > 3 versus MPC ≤ 3). (B) Burden of URVs evaluating missense variants with a more relaxed threshold (MPC > 2 versus MPC ≤ 2). In both panels, the left x-axis represents the excess of URVs per case (linear regression coefficient, β), and the right x-axis represents the corresponding odds ratio (OR). Points indicate the effect estimates derived from regression models adjusted for sex, the top five principal components, and total URV count, with error bars representing 95% confidence intervals. The vertical dashed line denotes an effect size of zero (β = 0, OR = 1). *P*-values are derived from the respective regression models.

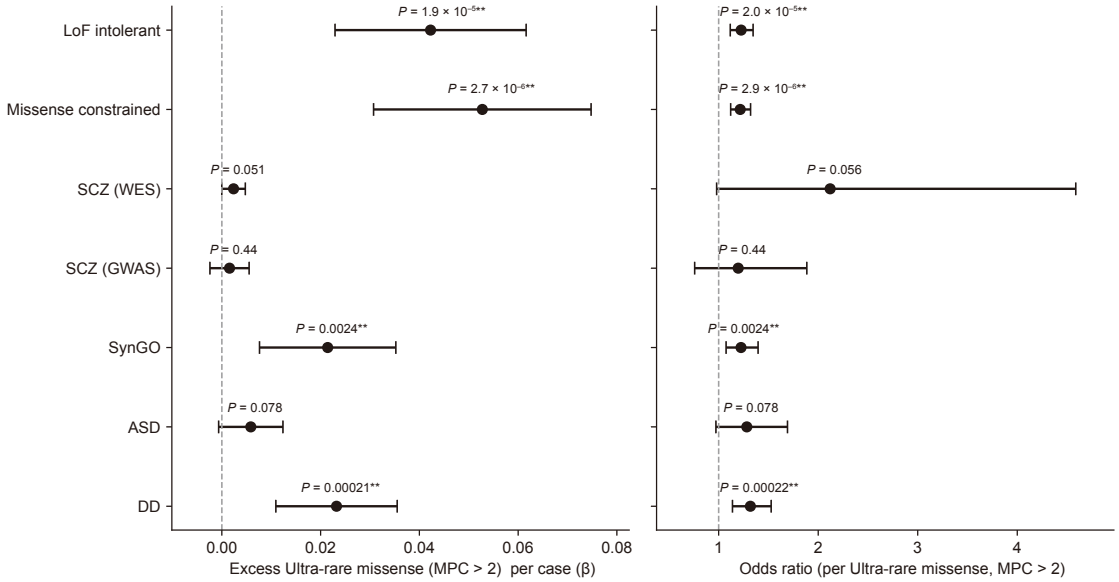

Supplementary Figure 5. Enrichment of ultra-rare damaging missense variants across functionally and genetically defined gene sets.

Burden of ultra-rare damaging missense variants (MPC > 2) alone in specific gene sets. The x-axis represents the excess of these variants per case (linear β, left) and the odds ratio (right). Evaluated gene sets include LoF intolerant genes (LOEUF < 0.35), missense constrained genes (Z-score > 3.09), previously implicated schizophrenia risk genes from WES (SCZ WES) and GWAS (SCZ GWAS), synaptic genes (SynGO), and genes implicated in autism spectrum disorder (ASD) and developmental disorders (DD). Points represent effect estimates with 95% confidence intervals (error bars). Statistical significance was assessed using regression models adjusted for sex, the top five principal components, and total URV count, with asterisks denoting the FDR-adjusted q-values (* $q < 0.05$, ** $q < 0.01$).

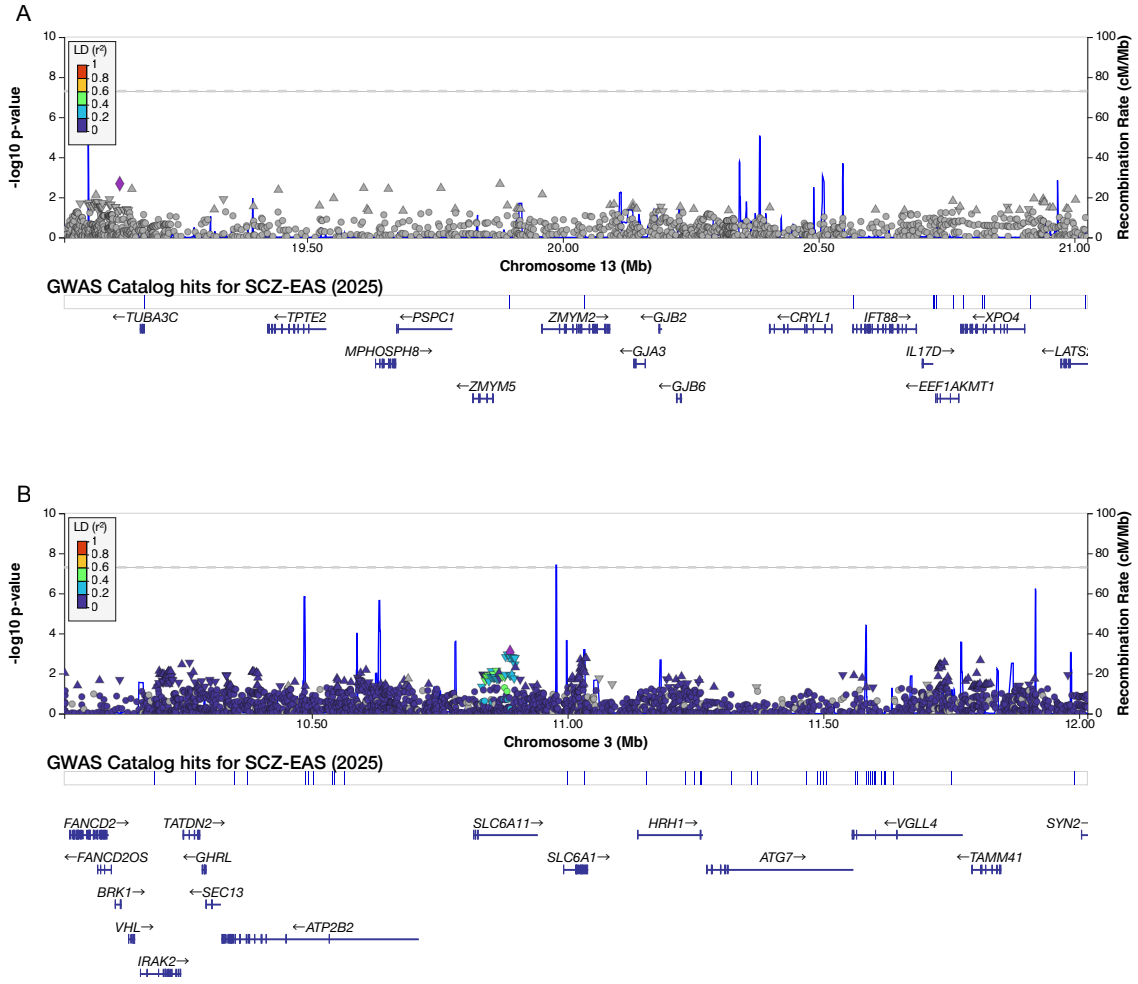

Supplementary Figure 6. Schizophrenia GWAS locus plots for *ZMYM2* and *SLC6A1*. Summary statistics for the recent East Asian (EAS) schizophrenia GWAS were visualized using LocusZoom (16). The left y-axis shows the -log10 *P*-values of each SNP from the EAS schizophrenia GWAS summary statistics (11), and the color of each symbol shows the linkage disequilibrium (LD, r^2) with the index single-nucleotide polymorphism (SNP). The right y-axis indicates the local recombination rate (blue line). Below the locus plots are the previously reported GWAS Catalog hits for East Asian schizophrenia and the gene annotations within the surrounding genomic regions of *ZMYM2* **(A)** and *SLC6A1* **(B)**.

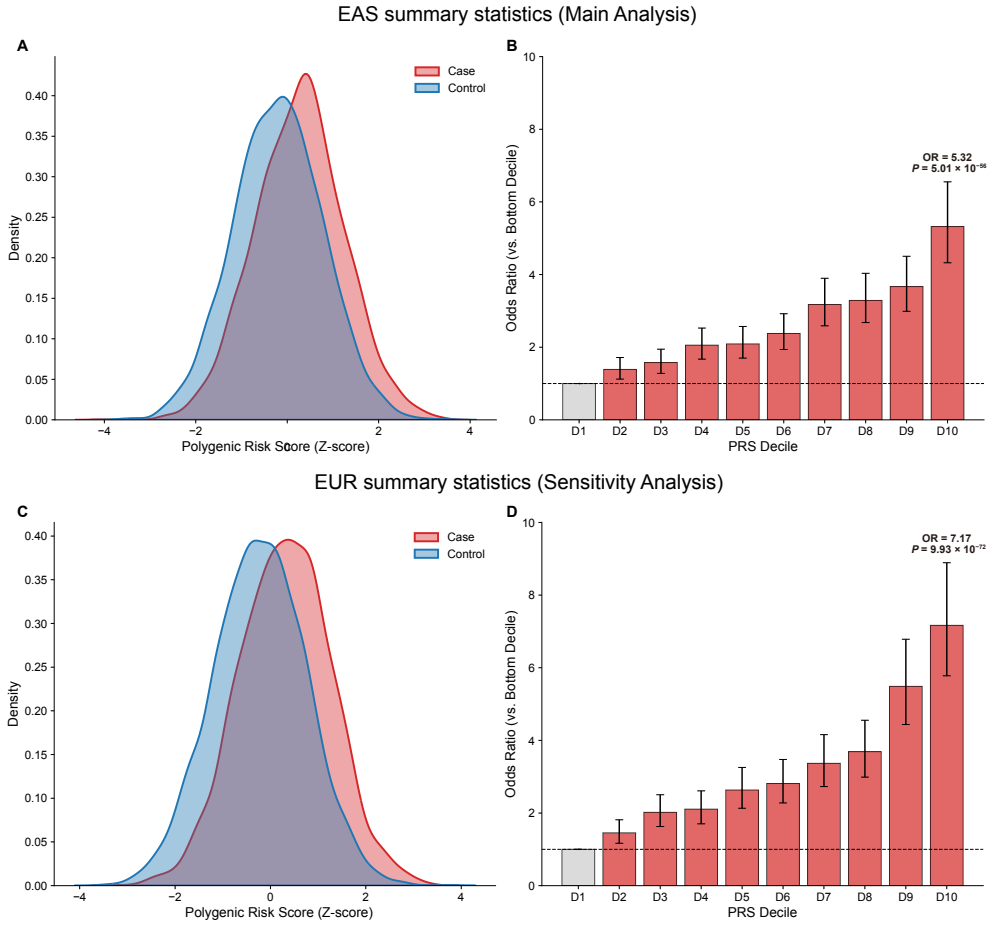

Supplementary Figure 7. Evaluation of Polygenic Risk Scores (PRS) across Different Base Summary Statistics.

(A, B) Evaluation of the primary PRS from the East Asian (EAS) summary statistics (10). **(A)** Density plot comparing the PRS distributions (Z-scores) between schizophrenia cases (red) and controls (blue). **(B)** Odds ratios for schizophrenia across PRS deciles (D1–D10) compared to the bottom decile (D1). The top decile (D10) confers a robust risk (OR = 5.32, $P = 5.01 \times 10^{-56}$). In a continuous logistic regression model, the EAS-PRS showed an OR per 1 SD of 1.63 ($P = 8.57 \times 10^{-95}$) and a full-model AUC of 0.67. **(C, D)** Sensitivity evaluation using an independent PRS derived from the European (EUR) summary statistics (11) to assess robustness to potential sample overlap. **(C)** Density plot for the EUR-derived PRS. **(D)** Odds ratios across EUR-PRS deciles. The top EUR-PRS decile (D10) had an OR of 7.17 ($P = 9.93 \times 10^{-72}$) relative to the bottom decile (D1). In a continuous model, the EUR-derived PRS showed an OR per 1 SD of 1.77 ($P = 4.20 \times 10^{-123}$) and a full-model AUC of 0.68.

Error bars represent 95% confidence intervals. All panels were based on 8,948 participants with available PRS data (3,829 cases and 5,119 controls).

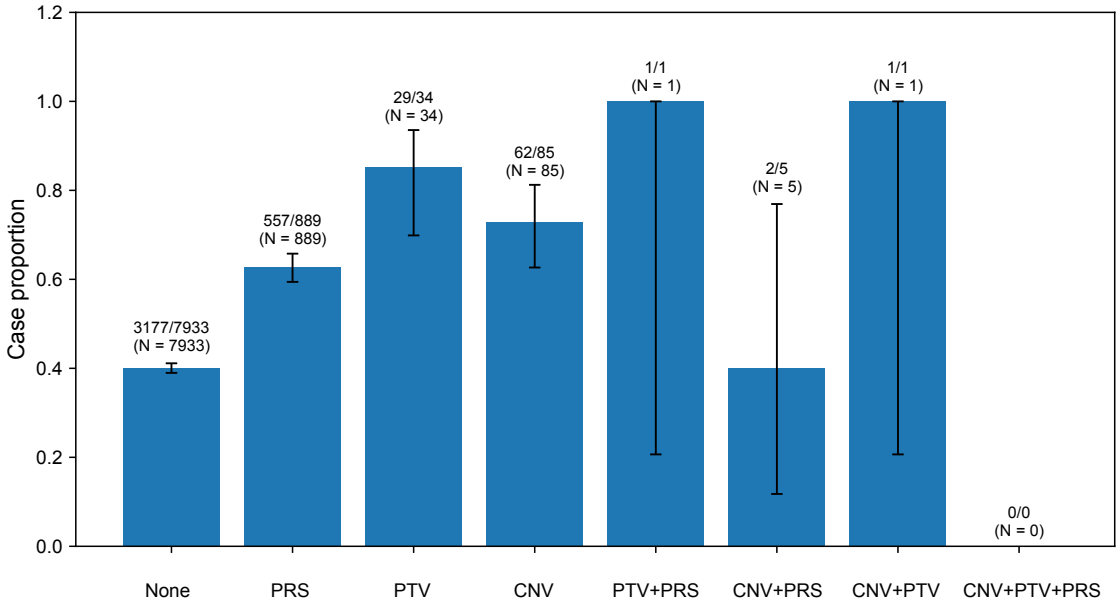

Supplementary Figure 8. Detailed case proportion across all combinations of genetic risk factors.

Bar plot illustrating the proportion of schizophrenia cases across all eight possible combinations of three binary risk factors evaluated in the joint analysis: pathogenic CNVs, known risk-gene PTVs, and top-decile of the primary PRS. Exact number of cases and the total number of individuals (N) for each combination are indicated above the respective bars. Error bars represent 95% confidence intervals calculated using the Wilson score interval. All panels were based on 8,948 participants with available PRS data (3,829 cases and 5,119 controls).

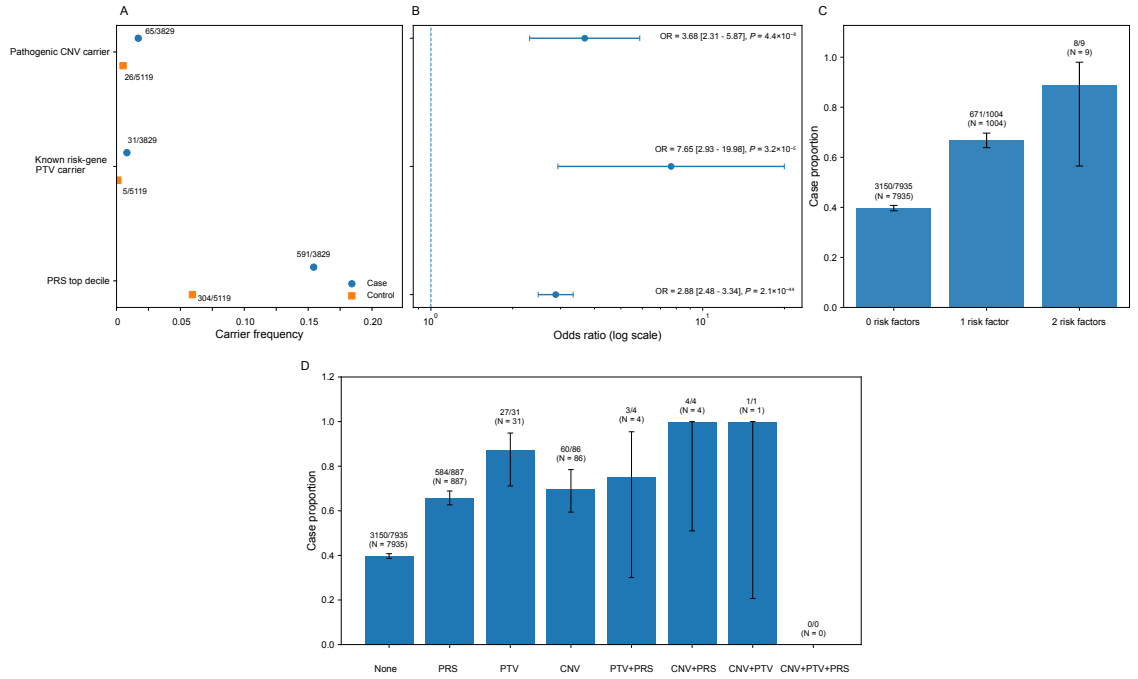

Supplementary Figure 9. Sensitivity analysis of the joint risk architecture using an independent European-derived polygenic risk score.

To assess the robustness of the findings to potential sample overlap, we repeated the joint analysis using an independently derived EUR PRS. This involved replacing the primary PRS with an independent PRS derived from EUR summary statistics. **(A)** Carrier frequencies of pathogenic CNVs, known risk-gene PTVs, and the top decile of EUR-derived PRS in schizophrenia. **(B)** Forest plot displaying ORs and 95% confidence intervals from a joint logistic regression model incorporating all three binary risk factors, adjusted for sex and the top five PCs. **(C)** Proportion of schizophrenia cases stratified by the cumulative number of genetic risk factors carried by an individual (0–2 risk factors). **(D)** Detailed case proportions across all eight possible combinations of the three risk factors. For panels C and D, the exact number of cases and total number of individuals (N) for each group are indicated above the respective bars. Error bars represent 95% confidence intervals calculated using the Wilson score interval. The broadly similar pattern observed with the EUR-derived PRS indicates that the findings were not restricted to the primary EAS-derived PRS analysis. All panels were based on 8,948 participants with available PRS data (3,829 cases and 5,119 controls).

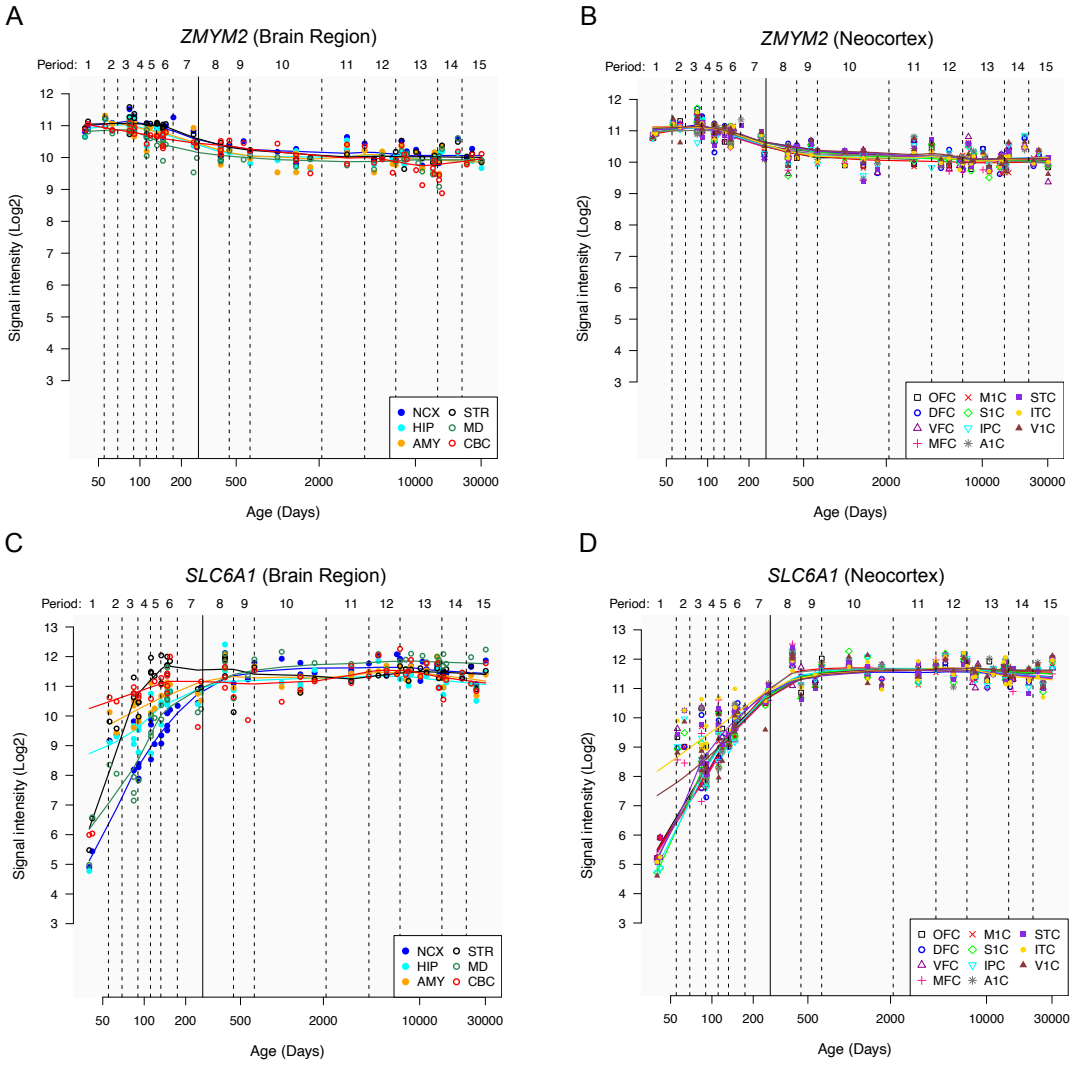

Supplementary Figure 10. Spatiotemporal expression profiles of *ZMYM2* and *SLC6A1* in the developing and adult human brain.

Longitudinal gene expression trajectories for *ZMYM2* (**A**, **B**) and *SLC6A1* (**C**, **D**) across various brain regions (**A**, **C**) and neocortical areas (**B**, **D**) as derived from the Human Brain Transcriptome (HBT) database (17). The y-axis represents the log2-transformed signal intensity from microarray data, and the x-axis developmental age in days (log scale). The developmental epochs (Periods 1–15) span from early embryonic stages (Periods 1–7; prenatal) to late adulthood (Periods 8–15; postnatal). *ZMYM2* predominantly exhibits high expression during early fetal neurodevelopment (prenatal periods) and gradually declines thereafter. Conversely, *SLC6A1* expression is minimal during the prenatal stages but dramatically rises postnatally and remains high throughout adulthood.

REFERENCES

1. Li H. A statistical framework for SNP calling, mutation discovery, association mapping and population genetical parameter estimation from sequencing data. Bioinformatics. 2011;27(21):2987-93.
2. Purcell S, Neale B, Todd-Brown K, Thomas L, Ferreira MA, Bender D, et al. PLINK: a tool set for whole-genome association and population-based linkage analyses. Am J Hum Genet. 2007;81(3):559-75.
3. Singh T, Poterba T, Curtis D, Akil H, Al Eissa M, Barchas JD, et al. Rare coding variants in ten genes confer substantial risk for schizophrenia. Nature. 2022;604(7906):509-16.
4. Chick SL, Holmans P, Cameron D, Grozeva D, Sims R, Williams J, et al. Whole-exome sequencing analysis identifies risk genes for schizophrenia. Nat Commun. 2025;16(1):7102.
5. Fromer M, Purcell SM. Using XHMM Software to Detect Copy Number Variation in Whole-Exome Sequencing Data. Curr Protoc Hum Genet. 2014;81:7 23 1-7 1.
6. Browning BL, Tian X, Zhou Y, Browning SR. Fast two-stage phasing of large-scale sequence data. Am J Hum Genet. 2021;108(10):1880-90.
7. Browning BL, Zhou Y, Browning SR. A One-Penny Imputed Genome from Next-Generation Reference Panels. Am J Hum Genet. 2018;103(3):338-48.
8. Chang CC, Chow CC, Tellier LC, Vattikuti S, Purcell SM, Lee JJ. Second-generation PLINK: rising to the challenge of larger and richer datasets. Gigascience. 2015;4:7.
9. Ge T, Chen CY, Ni Y, Feng YA, Smoller JW. Polygenic prediction via Bayesian regression and continuous shrinkage priors. Nat Commun. 2019;10(1):1776.
10. Trubetskoy V, Pardinas AF, Qi T, Panagiotaropoulou G, Awasthi S, Bigdeli TB, et al. Mapping genomic loci implicates genes and synaptic biology in schizophrenia. Nature. 2022;604(7906):502-8.
11. Bigdeli TB, Chatzinakos C, Bendl J, Barr PB, Venkatesh S, Gorman BR, et al. Biological insights into schizophrenia from ancestrally diverse populations. Nature. 2026;651(8105):404-13.
12. Cuinat S, Nizon M, Isidor B, Stegmann A, van Jaarsveld RH, van Gassen KL, et al. Loss-of-function variants in SRRM2 cause a neurodevelopmental disorder. Genet Med. 2022;24(8):1774-80.
13. Fenster SD, Chung WJ, Zhai R, Cases-Langhoff C, Voss B, Garner AM, et al. Piccolo, a presynaptic zinc finger protein structurally related to bassoon. Neuron. 2000;25(1):203-14.
14. Gundelfinger ED, Reissner C, Garner CC. Role of Bassoon and Piccolo in Assembly and Molecular Organization of the Active Zone. Front Synaptic Neurosci. 2015;7:19.
15. Furukawa S, Kushima I, Kato H, Kimura H, Nawa Y, Aleksic B, et al. Whole-genome sequencing analysis of Japanese autism spectrum disorder trios. Psychiatry Clin Neurosci.

2025;79(3):87-97.
16. Boughton AP, Welch RP, Flickinger M, VandeHaar P, Taliun D, Abecasis GR, et al. LocusZoom.js: interactive and embeddable visualization of genetic association study results. Bioinformatics. 2021;37(18):3017-8.
17. Kang HJ, Kawasawa YI, Cheng F, Zhu Y, Xu X, Li M, et al. Spatio-temporal transcriptome of the human brain. Nature. 2011;478(7370):483-9.